Detection of Oxygenated Aromatics in Atmospheric Anisole Flames

Kanika Sood, Sylvie Gosselin, Juan Carlos Lizardo Huerta, Abderrahman El Bakali, Mehrdad Seifali Abbas-Abadi, Nathalie de Coensel, Kevin M van Geem, Laurent Gasnot, Luc-Sy Tran

Detection of Oxygenated Aromatics in Atmospheric Anisole Flames

K. Sood[1], S. Gosselin[1], J.-C. Lizardo-Huerta[1], A. El Bakali[1], M.S. Abbas-Abadi[2], N. De Coensel[2], K. M. Van Geem[2], L. Gasnot[1], L.-S. Tran*[1]

[1] Univ. Lille, CNRS, UMR 8522 - PC2A - Physicochimie des Processus de Combustion et de l'Atmosphère, F-59000 Lille, France.

[2] Laboratory for Chemical Technology (LCT), Ghent University, Technologiepark 125, B-9052 Ghent, Belgium.

Abstract

Despite the undeniable interest presented by biofuels, their combustion processes are likely to modify the formation of aromatic species, especially oxygenated aromatics, that may profoundly modify the properties of the formed soot particles. However, the kinetics of oxygenated aromatics are not well studied yet. In this work, a laminar premixed flame of anisole (a surrogate for lignin-based biofuels) and hydrocarbon fuel blend was investigated under fuel-rich conditions. Chemical products sampled from the flames were analyzed using 1D and 2D Gas Chromatography that have enabled us to separate and identify around 100 aromatic species including 60 oxygenated ones with different functional groups (alcohols, ethers, aldehydes, ketones, esters, acids).

Keywords: flames, biofuel, anisole, oxygenated aromatics, kinetics.

Introduction

Around 80% of the energy production comes from the combustion of fossil fuels. Research interests have shifted towards exploring environment friendly alternative fuels with the intercontinental awareness and recognition of energy and environmental concerns. Biofuels are being considered as a vital part of sustainable energy panel, where they promise to contribute to our society's energy security [1,2]. Despite the undeniable interest presented by these biofuels, their combustion processes are likely to modify the formation of aromatic species, especially oxygenated aromatics, that may profoundly modify the properties of the formed soot particles [3]. Recent studies have illustrated the acute challenges associated with the experimental identification of such isomeric oxygenated aromatics, whereas this information is somewhat crucial for decoding their formation kinetics [4]. In this work, anisole has been chosen as an effortless model compound for lignin-based biofuels. It is also a worthy biofuel candidate owing to its suitable properties, for instance, its high-octane number and a superior net heating value than ethanol.

Experimental methods

A laminar premixed flame burner and different Gas Chromatography (GC) setups were used to carry out this work (Fig. 1). These setups have been described in the subsequent sections.

Flame burner setup:

A flame of iso-octane (C_8H_{18})/methane (CH_4) doped with 10% anisole (in mole) was stabilized at atmospheric pressure on a McKenna flat flame burner which consists of a central bronze porous plug (60 mm in diameter). The porous zone is surrounded by another co-annular porous used for the nitrogen shroud (25 nL/min), which protects the flame from air entrainment responsible for the formation of any peripheral diffusion flame and aerodynamic perturbations. The temperature of the burner is constantly maintained at 60°C using a cryostat. In order to stabilize fuel-rich flames, a stainless-steel disc, also known as the stagnation plate (6 cm in diameter and 3 cm thick) was surmounted at a distance of 21 mm with respect to the burner surface and is pierced at its center to provide access for the quartz microprobe. An additional metallic grid was placed directly on the stagnation plate, to avoid peripherical flame ignition.

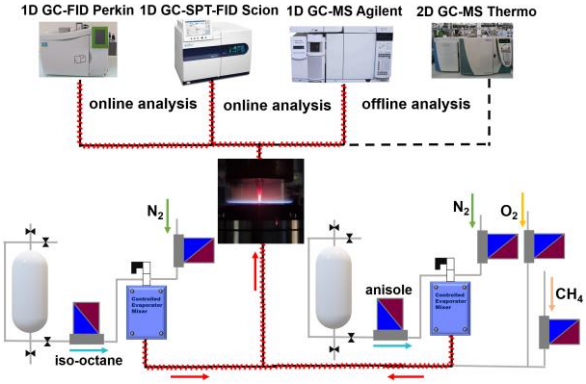

Fig. 1. Experimental setup of premixed flame burner.

A gas sample was extracted from the flame and directed to the sampling line via a quartz microprobe with an orifice diameter of about 180 micrometers. The burner could be vertically displaced with respect to the microprobe in order to effectuate the sampling process at different heights above the burner (HAB). Thereafter, the sample is sent to the GC loops. This sampling procedure is done as fast as possible.

The liquid flow rate of anisole (Sigma-Aldrich, purity 99.7%) was controlled using a Coriolis flow controller (Bronkhorst, error ±0.2%) followed by an evaporator/mixer, in which anisole is vaporized and

* Corresponding author: luc-sy.tran@univ-lille.fr

mixed with N_2. The gaseous stream is then mixed with O_2 and CH_4 and fed to the burner. Flow rates of CH_4 (Air Liquide, purity ≥99.95%), O_2 (Air Liquide, purity ≥99.995%) and N_2 (Air Liquide, purity ≥99.995%) were controlled using mass flow controllers (Bronkhorst, error ±0.5%). Some parameters of the investigated flame are listed in Table. 1.

Table. 1. Flame conditions for the investigated flame

Φ	Anisole in fuel (%)	Mole fraction				
		C_8H_{18}	Anisole	CH_4	O_2	N_2
1.9	10	0.015	0.01	0.08	0.23	0.66

GCs:

Aromatics were identified by both their individual retention times and MS (Mass Spectroscopy) spectra, which were obtained from three 1D GCs at PC2A and one 2D GC at LCT (University of Ghent).

The first 1D GC (GC Perkin Elmer Clarus 580) device comprises of a capillary column Rt-Q Bond (30 m × 0.25 mm × 0.08 mm, 100% divinylbenzene, Restek) using helium as the carrier gas and a Flame Ionization Detector (FID) equipped with a methanizer. This system enabled us to analyze several lighter hydrocarbons, oxygenated species and monoaromatics (benzene, cresols, etc.).

A second GC (GC-Scion 456) equipped with the SPT (Sample Pre-concentration Trap) system is used. This concentrating system operates on the idea of cryofocusing–thermodesorption which is a common and a very powerful technique to perform low level determinations. In order to preconcentrate analytes within the SPT system, the gaseous flame sample is preconcentrated on inert adsorptive glass beads at a specific adsorption temperature (-50°C) using a coolant (liquid N_2). Through subsequent rapid heating of the adsorptive material to a desorption temperature (200°C), the steady state is instantaneously shifted towards desorption (thermodesorption), consequently remobilizing the trapped analytes. Formerly trapped analytes are then flushed in the opposite direction to sampling flow, onto the chromatographic column (SCION-17MS; 30 m × 0.32 mm × 0.25 μm, 50% phenyl methylpolysiloxane) with helium as the carrier gas for separation and detected with the FID detector.

A third 1D GC equipped with a mass spectrometer (MS) with electron ionization at 70 eV (Agilent Technologies 5975C). Two columns were alternatively used, which are Rt-Q Bond and SCION-17MS (same as those used in the two GCs above). Analyses were performed online (for small aromatics) and offline using a liquid N_2 system (for heavy aromatics). The obtained mass spectrum was compared with spectral libraries from NIST.

A fourth GC is a 2D GC-MS (Thermo Scientific Trace GC Ultra, with Quadrupole Mass Analyzer with electron ionization at 70 eV) at LCT (University of Ghent). The trapped liquid samples were analyzed using this GC. This GC apparatus exploits two different stationary phases in two different columns: a non-polar column (DB-5MS; 30 m × 0.25 mm × 0.25 μm) and a polar column (DB-17MS; 2 m × 0.25 mm × 0.25 μm) in the same oven using helium as the carrier gas. A two-jet cryogenic modulator (liquid CO_2) is placed between the two columns and its functions are to trap, isolate, focus and reinject the bands of the eluate from the first column in the second column. The exhaustive transfer of a primary dimension eluting peak into the secondary column can be achieved with an appropriate modulation time (6 seconds in this study). Such a separation mechanism makes 2D GC having an enhanced resolution. The analysis from 2D GC has added further information on detection of aromatic species.

Results and discussions

Example of obtained chromatograms and mass spectra:

Representative chromatograms and mass spectra are shown in Fig. 2. The middle panel of this figure presents two chromatograms obtained via the 1D GC (on the left) and the 2D GC (on the right). The columns used for these GC devices are specific to aromatic species. Despite being very complex, the 1D GC chromatogram consisting of about 120 peaks indicates that several aromatic species are present in the anisole flame. Several peaks amongst these have been identified using 1D GC-MS and we observed that so far about 50% of these aromatics are oxygenated (60 species), which highlights their significant co-formation with classic aromatics. Following the complexity of the 1D GC chromatogram, we chose to perform additional analyses using the 2D GC-MS. By using the 2D GC-MS, we could confirm the identification from 1D GC-MS as well as identify additional species apart from the ones already identified from 1D GC-MS on account of its increased separation capacity. For example, dibenzofuran ($C_{12}H_8O$) and bis(2-hydroxyphenyl) methane ($C_{13}H_{12}O_2$) identified by 1D GC-MS were confirmed by 2D GC-MS.

The top and bottom panels of Fig. 2 show the mass spectra of these two species and other four selected oxygenated aromatics. The presence of the molecular ion peaks (base peak) and fragment peaks in these spectra are very consistent with the molecular mass and the fragmentation mechanism of the identified molecules. An example of the anticipated fragmentation pattern for 4-methylphenyl acetate is shown in Fig. 3. The peak at m/z 150 corresponds to the mass of 4-methylphenyl acetate. This molecule can readily undergo the benzyl ester rearrangement by eliminating a ketene molecule in order to form this fragment ion at m/z 108 (see path 1). This phenolic molecular ion fragment may further preferably dissociate via the benzylic H-bond cleavage to produce another intense peak at m/z 107. This resonance stabilized benzyl ion may reversibly isomerize to the corresponding tropylium ion isomers m/z 107 (see path 2).

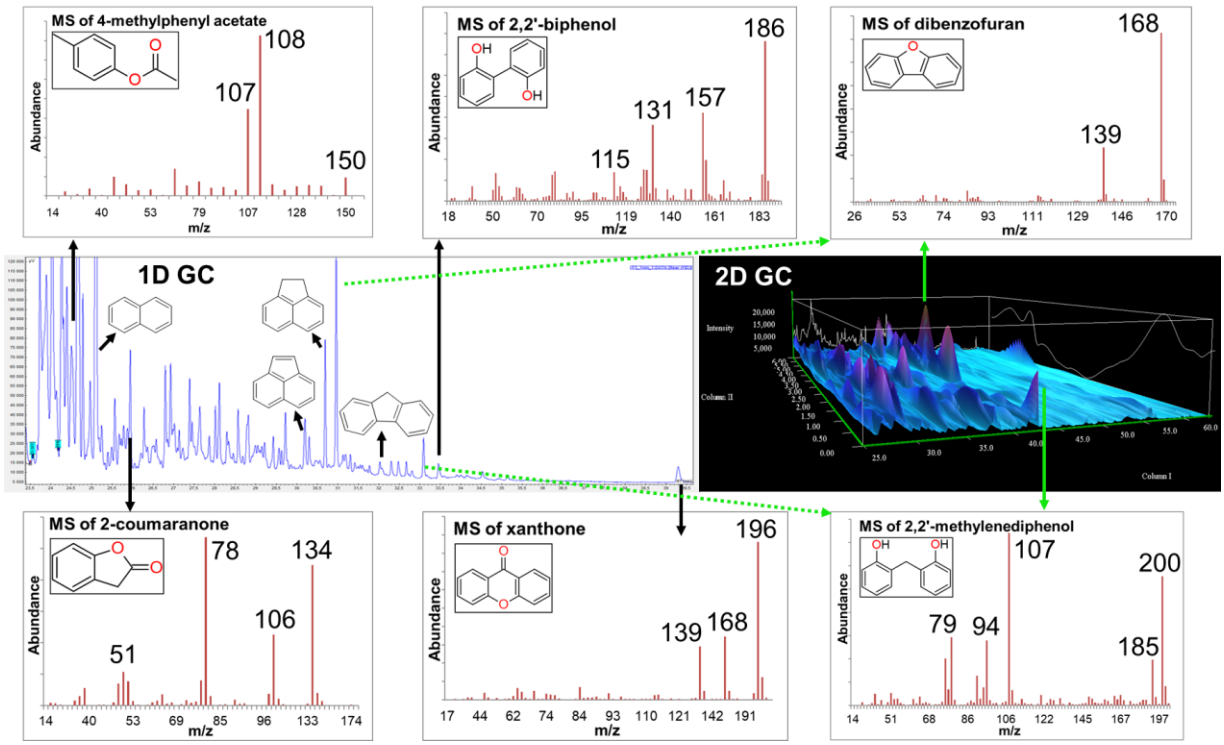

Fig. 2. Examples of chromatograms (middle panel) obtained by 1D and 2D GCs in the doped anisole flame at HAB=1.5 mm. The nomenclature of some important species is given. Some mass spectra (MS, top and bottom panels) for the selected oxygenated aromatics obtained by GC-MS are presented.

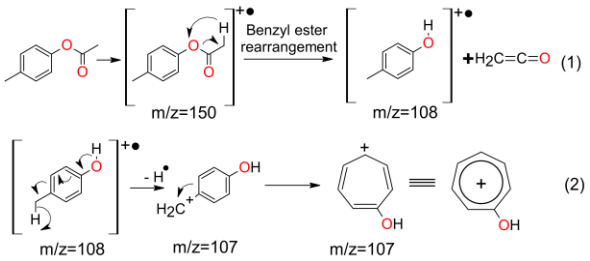

Fig. 3. Example of fragmentation rules used to explain the mass spectra of 4-methylphenyl acetate.

Identified oxygenated aromatics:

Based on the above described approach, about 60 oxygenated mono- and poly-cyclic aromatics were identified. They are reported in Table. 2 with their molar mass, formula, names and structures. These species have molar masses ranging from 94 (phenol, C_6H_6O) to 226 (xanthene-9-carboxylic acid, $C_{14}H_{10}O_3$) and contain in their structure one to three oxygen atoms. More than half of the detected species (e.g. xanthene, xanthone etc.) are reported for the first time for anisole combustion. The employed GC setup allowed us to distinguish between several different isomers such as C_7H_8O (mass 108, 4 isomers), $C_{10}H_8O$ (mass 144, 4 isomers), $C_{13}H_{10}O$ (mass 182, 4 isomers). Also, species with the same nominal mass were also well separated, such as 6 species at mass 122, 5 species at mass 184, 5 species at mass 186. Separating and identifying these species is known to be very challenging when using the time-of-flight mass spectrometry (Tof-MS) technique in [4–6].

The detected oxygenated aromatics contain different functional groups: alcohols, ethers, carbonyls (aldehydes, ketones), esters, and acids. The numbers of groups are counted and summarized in Fig. 4. Alcohols and ethers are predominant (25 and 23 species, respectively). The abundance of ethers could be consistent with the chemical structure of the fuel (anisole, an ether). But interestingly, 15 amongst 23 ethers are cyclic ethers (O atom in the cycle) whereas anisole itself is not a cyclic ether. The abundance of alcohols (25 species) indicates that the conversion of the ether fuel to alcoholic products is an important process under the studied conditions.

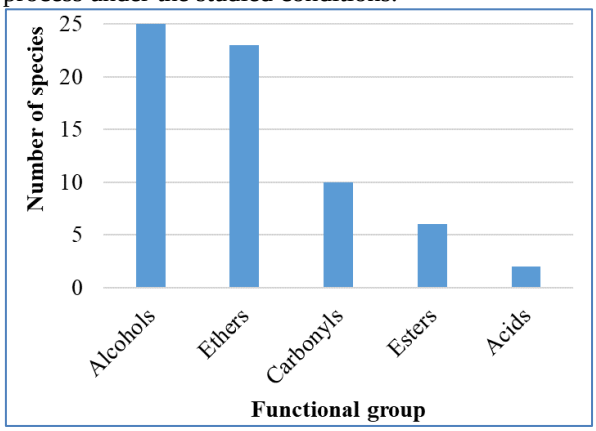

Fig. 4. Number of oxygenated aromatics with different functional groups. Carbonyls include aldehydes and ketones.

Table. 2. Identified oxygenated aromatics. When several names are given, the second name is the IUPAC one. M: Nominal mass. Bold M indicates isomeric structures.

M	Formula	Name [a]	Structure
94	C_6H_6O	Phenol	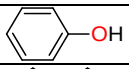
106	C_7H_6O	Benzaldehyde	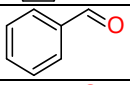
108	C_7H_8O	Anisole	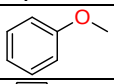
	C_7H_8O	*o*-Cresol; *2-Methylphenol*	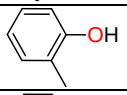
	C_7H_8O	*m*-Cresol; *3-Methylphenol*	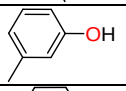
	C_7H_8O	*p*-Cresol; *4-Methylphenol*	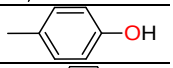
110	$C_6H_6O_2$	Hydroquinone; *Benzene-1,4-diol*	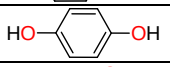
118	C_8H_6O	Benzofuran; *1-Benzofuran*	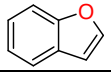
120	C_8H_8O	2,3-Dihydrobenzofuran; *2,3-Dihydro-1-benzofuran*	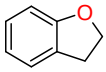
122	$C_7H_6O_2$	Salicylaldehyde; *2-Hydroxybenzaldehyde*	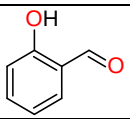
	$C_7H_6O_2$	*m*-Formylphenol; *3-Hydroxybenzaldehyde*	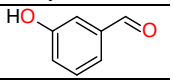
	$C_7H_6O_2$	1,3-Benzodioxole; *2H-1,3-benzodioxole*	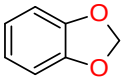
	$C_8H_{10}O$	Ethyl phenyl ether; *Ethoxybenzene*	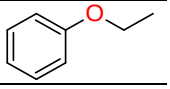
	$C_8H_{10}O$	2,6-Xylenol; *2,6-Dimethylphenol*	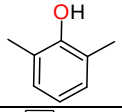
	$C_8H_{10}O$	2-Ethyl phenol	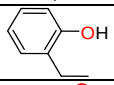
124	$C_7H_8O_2$	*m*-Guaiacol; *3-Methoxyphenol*	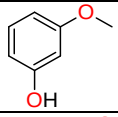
132	C_9H_8O	1-Indanone; *2,3-Dihydro-1H-inden-1-one*	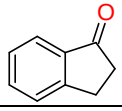
	C_9H_8O	Cinnamaldehyde; *(2E)-3-Phenylprop-2-enal*	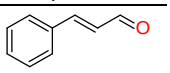
	C_9H_8O	2-Methyl benzofuran; *2-Methyl-1-benzofuran*	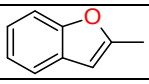
134	$C_8H_6O_2$	2-Coumaranone; *1-Benzofuran-2(3H)-one*	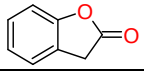
136	$C_8H_8O_2$	*p*-Toluic acid; *4-Methylbenzoic acid*	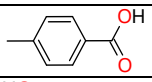
	$C_9H_{12}O$	5-Ethyl *m*-cresol; *3-Ethyl-5-methylphenol*	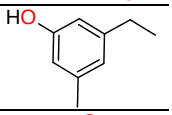
144	$C_{10}H_8O$	2-Vinyl benzofuran; *2-Ethenyl-1-benzofuran*	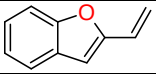
	$C_{10}H_8O$	1-Naphthol; *Naphthalen-1-ol*	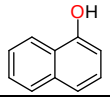
	$C_{10}H_8O$	2-Naphthol; *Naphthalen-2-ol*	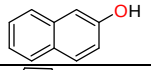
	$C_{10}H_8O$	3-Phenylfuran	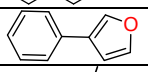
146	$C_{10}H_{10}O$	1-Methylindan-2-one; *1-Methyl-1,3-dihydro-2H-inden-2-one*	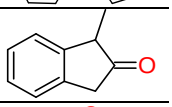
	$C_{10}H_{10}O$	2-Ethyl benzofuran; *2-Ethyl-1-benzofuran*	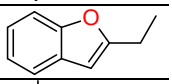
150	$C_9H_{10}O_2$	*o*-Acetoxy toluene; *2-Methylphenyl acetate*	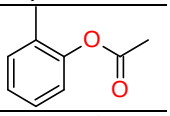
	$C_9H_{10}O_2$	*p*-Acetoxy toluene; *4-Methylphenyl acetate*	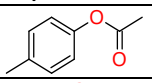
	$C_9H_{10}O_2$	Phenyl propionate; *Phenyl propanoate*	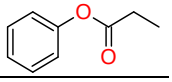
156	$C_{11}H_8O$	2-Naphthaldehyde; *Naphthalene-2-carbaldehyde*	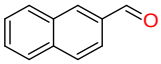
162	$C_{11}H_{14}O$	2,2-dimethyl-3,4-dihydro-2*H*-1-Benzopyran	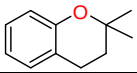
168	$C_{12}H_8O$	Dibenzofuran; *Dibenzo[b,d]furan*	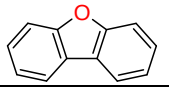
170	$C_{12}H_{10}O$	Diphenyl ether; *1,1'-Oxydibenzene*	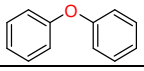
	$C_{12}H_{10}O$	*o*-Hydroxybiphenyl; *[1,1'-Biphenyl]-2-ol*	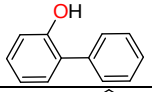
	$C_{12}H_{10}O$	1-Naphthyl vinyl ether; *1-(Ethenyloxy)naphthalene*	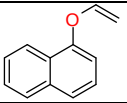
180	$C_{13}H_8O$	9-Fluorenone; *9H-Fluoren-9-one*	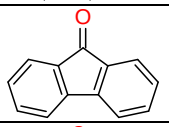
182	$C_{13}H_{10}O$	Xanthene; *9H-Xanthene*	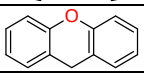
	$C_{13}H_{10}O$	9-Fluorenol; *9H-fluoren-9-ol*	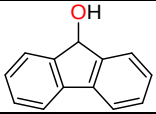
	$C_{13}H_{10}O$	4-Methyldibenzo[*b,d*]furan	

	$C_{13}H_{10}O$	6*H*-Dibenzo[*b*,*d*]pyran	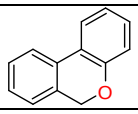
184	$C_{12}H_8O_2$	Dibenzo-p-dioxin; *Oxanthrene*	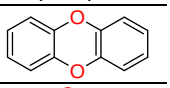
	$C_{12}H_8O_2$	2-Dibenzofuranol; *Dibenzo[b,d]furan-2-ol*	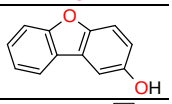
	$C_{13}H_{12}O$	Benzyl phenyl ether; *(Benzyloxy)benzene*	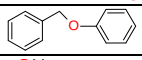
	$C_{13}H_{12}O$	*o*-Benzylphenol; *2-Benzylphenol*	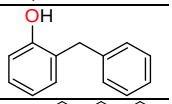
	$C_{13}H_{12}O$	*p*-Benzylphenol; *4-Benzylphenol*	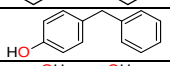
186	$C_{12}H_{10}O_2$	2,2′-Diphenol; *[1,1'-Biphenyl]-2,2'-diol*	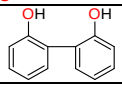
	$C_{12}H_{10}O_2$	m-Phenoxy phenol; *3-Phenoxyphenol*	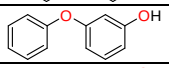
	$C_{12}H_{10}O_2$	1-Naphthyl acetate; *Naphthalen-1-yl acetate*	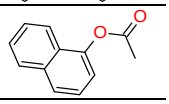
	$C_{13}H_{14}O$	2-(2-Naphthyl)-2-propanol; *2-(Naphthalen-2-yl)propan-2-ol*	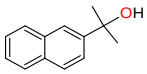
	$C_{13}H_{14}O$	2,5,8-Trimethylnaphthalen-1-ol	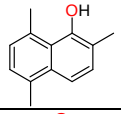
196	$C_{13}H_8O_2$	Xanthone; *9H-Xanthen-9-one*	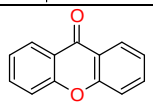
198	$C_{14}H_{14}O$	1,2,3,4-tetrahydrophenanthren-4-ol	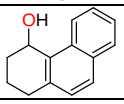
200	$C_{13}H_{12}O_2$	Bis(2-hydroxyphenyl) methane; 2,2'-*Methylenediphenol*	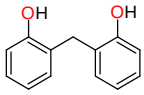
	$C_{13}H_{12}O_2$	2-[(4-Hydroxyphenyl) methyl] phenol	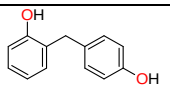
208	$C_{14}H_8O_2$	Anthraquinone; *Anthracene-9,10-dione*	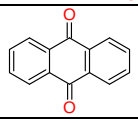
212	$C_{15}H_{16}O$	1,1-Diphenyl-1-methoxyethane; *1,1'-(1-Methoxyethane-1,1-diyl)dibenzene*	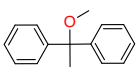
224	$C_{15}H_{12}O_2$	9-Fluorenyl acetate; *9H-Fluoren-9-yl acetate*	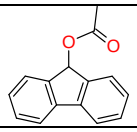
226	$C_{14}H_{10}O_3$	Xanthene-9-carboxylic acid; *9H-Xanthene-9-carboxylic acid*	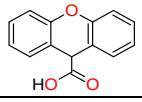

Possible formation pathways:

Some possible formation pathways for selected oxygenated aromatics from anisole are presented in Fig. 5. Addition of the OH radicals on the double bonds of the benzene ring (of anisole or of the subsequent products) could be one of the possible mechanisms contributing to the formation of alcoholic aromatics. The O–CH_3 bond in the methoxy group of anisole has a very low bond dissociation energy (63.2 kcal/mol), owing to which its unimolecular scission to yield phenoxy (C_6H_5O) and methyl (CH_3) radicals is strongly favored, especially under fuel-rich conditions [6]. Eventually, the resonance stabilized phenoxy radicals may react to form different oxygenated aromatics. For example, they could recombine with H atoms to form phenol [7] and with C_2H_2 to form benzofuran (C_8H_6O, mass 118) [5,8]. The latter may also be produced via H-atom abstraction from cresol, producing hydroxybenzyl and methylphenoxy radicals. These two radicals can isomerize to each other via an intermolecular H-transfer reaction. The recombination reaction between hydroxybenzyl radical and methyl radical could produce ethylphenol, which can then undergo a stepwise dehydrogenation reaction thereby forming ethenylphenol. The subsequent H-elimination from ethenylphenol produces ethenylphenoxy radical, which can proceed to an intermolecular cyclization reaction and then an H-elimination reaction to form benzofuran. [5]. The phenoxy radicals may also undergo self-recombination reactions followed by subsequent intramolecular rearrangements which may adequately elucidate the formation pathway to produce dibenzofuran ($C_{12}H_8O$, mass 168) [5,9] and dibenzo-p-dioxin ($C_{12}H_8O_2$, mass 184) [9]. Besides these pathways, benzofuran may also undergo H-abstraction and C_2H_2 addition reactions, consequently contributing to the formation of dibenzofuran [8]. Furthermore, anisole itself may undergo H-atom abstraction on the methoxy group by a H-atom, methyl, phenyl, and phenoxy radicals in order to yield the anisyl ($C_6H_5OCH_2$) radicals. This anisyl radical can isomerize to the benzoxyl ($C_6H_5CH_2O$) radical via the *ipso* rearrangement and then undergo the β-scission reaction to yield benzaldehyde (C_6H_5CHO, mass 106) [7]. Additionally, formation of guaiacol ($HOC_6H_4OCH_3$, mass 124) may arise directly from the fuel by *ipso* addition of hydroxyl radicals to anisole followed by the subsequent H-abstraction reaction [6].

Note that the formation of OPAHs from classical PAHs cannot be completely neglected. However, this contribution could be less significant as compared to the direct formation pathways from anisole as a flame without anisole and at similar conditions (equivalence ratio, total flow, dilution, etc.) was also investigated simultaneously and none of the OPAHs were observed in significant amounts. Thus, we may deduce that the OPAHs detected in the anisole doped flame are mainly produced from the added anisole.

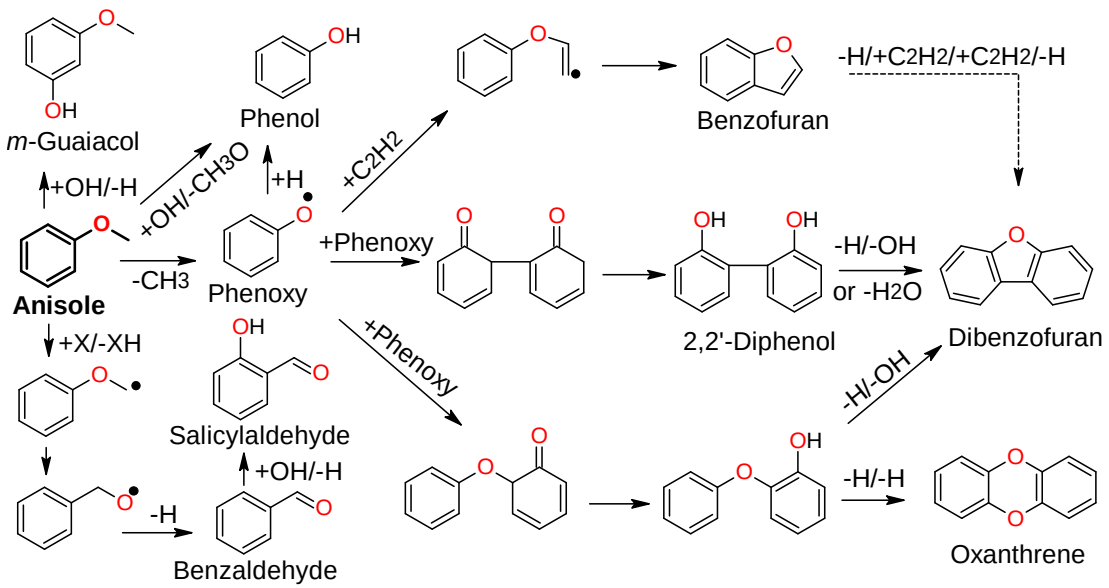

Fig. 5. Possible formation pathways of some selected oxygenated aromatics from anisole.

Conclusion and perspectives

The aromatic ring in anisole in combination with the methoxy group makes it the simplest model compound for lignin. The formation of oxygenated aromatics from anisole in laminar atmospheric premixed flames is investigated by using 1D and 2D GC systems. Several oxygenated aromatics have been identified in this work. Some of the species have been reported for the first time and can give us several insights about the kinetics of anisole in the flame conditions. These species would allow us to link several primary reactions with the formation of pollutants and potential soot particles formed during the combustion of lignin-derived surrogate biofuels. The next step is to analyze quantitatively these species and study their impact on soot formation, which is currently an ongoing project at our laboratory.

Acknowledgments

The authors would like to thank ADEME (The French Agency for the Ecological Transition) and the Hauts-de-France Region for their financial support. The work was funded by the support from I-SITE via the Biofuel-Soot project (R-JEUNES CHERCHEURS-19-010-TRAN). The support from IREPSE (L'Institut de Recherches Pluridisciplinaires en Sciences de l'Environnement) is also appreciated. The work was further supported by the French Ministère de l'Enseignement Supérieur et de la Recherche and the European Funds for Regional Economic Development for their financial support via the CPER research project CLIMIBIO.

References

[1] Leitner W, Klankermayer J, Pischinger S, Pitsch H, Kohse-Höinghaus K. Advanced biofuels and beyond: Chemistry solutions for propulsion and production. Angew Chem-Int Edit 2017;56:5412–52.

[2] Tran L-S, Herbinet O, Carstensen H-H, Battin-Leclerc F. Chemical kinetics of cyclic ethers in combustion. Progress in Energy and Combustion Science 2022;92:101019.

[3] Guan C, Cheung CS, Li X, Huang Z. Effects of oxygenated fuels on the particle-phase compounds emitted from a diesel engine. Atmospheric Pollution Research 2017;8:209–20.

[4] Chen B, Kruse S, Schmid R, Cai L, Hansen N, Pitsch H. Oxygenated PAH Formation Chemistry Investigation in Anisole Jet Stirred Reactor Oxidation by a Thermodynamic Approach. Energy Fuels 2020.

[5] Yuan W, Li T, Li Y, Zeng M, Zhang Y, Zou J, et al. Experimental and kinetic modeling investigation on anisole pyrolysis: Implications on phenoxy and cyclopentadienyl chemistry. Combustion and Flame 2019;201:187–99.

[6] Bierkandt T, Hemberger P, Oßwald P, Krüger D, Köhler M, Kasper T. Flame structure of laminar premixed anisole flames investigated by photoionization mass spectrometry and photoelectron spectroscopy. Proceedings of the Combustion Institute 2019;37:1579–87.

[7] Nowakowska M, Herbinet O, Dufour A, Glaude P-A. Detailed kinetic study of anisole pyrolysis and oxidation to understand tar formation during biomass combustion and gasification. Combust Flame 2014;161:1474–88.

[8] Shi X, Wang Q, Violi A. Chemical pathways for the formation of benzofuran and dibenzofuran in combustion. Combust Flame 2020;212:216–33.

[9] Wiater I, Born JGP, Louw R. Products, rates, and mechanism of the gas-phase condensation of phenoxy radicals between 500-840 K. European Journal of Organic Chemistry 2000:921–8.